A General Kinetostatic Model Based Stiffness Estimation for Tripod Parallel Kinematic Machines with Prismatic Actuators

Jun Zhang and Tengfei Tang

Abstract A general stiffness modeling methodology for tripod parallel kinematic machines (PKMs) with prismatic actuators is proposed in this paper. With the technique of substructure synthesis, the whole system of a tripod is divided into a platform, a base and three kinematic limb substructures. Each limb assemblage is modeled as a spatial beam constrained by two sets of six degree-of-freedom (6-DOF) virtual lumped springs with equivalent stiffness at their geometric centers. The equilibrium equation of each individual limb assemblage is derived through finite element formulation, while that of the platform is derived with the Newton's 2nd law. The governing stiffness matrix is synthesized by introducing the deformation compatibility conditions between the platform and the limbs. By extracting a 6x6 block matrix from the inversion of the governing compliance matrix, a stiffness matrix of the platform is formulated. Taking the Sprint Z3 Head and the A3 Head as examples, the distributions of stiffness values of these two types of PKM modules are predicted and discussed. It is worth mentioning that the proposed methodology of stiffness modeling can further be applied to other types of PKMs for evaluating the global rigidity performance over entire workplace efficiently with minor revisions.

Keywords Parallel kinematic machine · Tripod · Kinetostatic · Stiffness modeling · Substructure synthesis

1 Introduction

Thanks to the merits of better accuracy and higher rigidity, the tripod parallel kinematic machines (PKMs) with prismatic actuators have been proved as a promising alternative solution for high speed machining (HSM) tasks on extra large

J. Zhang (✉)
School of Mechanical Engineering and Automation, Fuzhou University, Fuzhou, China
e-mail: zhang_jun@fzu.edu.cn

T. Tang
School of Mechanical Engineering, Anhui University of Technology, Ma'anshan, China

L. Yao et al. (eds.), *Advanced Mechanical Science and Technology for the Industrial Revolution 4.0*, https://doi.org/10.1007/978-981-10-4109-9_8

scale components with complex geometries. As a successful example, the Sprint Z3 head has been commercially applied in the aeronautical industries [1, 2]. Another newly invented and commercially applied tripod PKM is the Exechon, with an over-constrained 2UPR/1SPR topological architecture [3, 4]. Herein, 'R' and 'S' denote a revolute joint and a spherical joint respectively while 'P' represents an active prismatic joint. Inspired by the 3-PRS topology of the Sprint Z3 head, a similar 3-RPS tripod-based PKM named the A3 head was proposed as a multiple-axis spindle head to form a hybrid 5-axis high-speed machining unit [5, 6]. Other investigations on the tripod PKMs can also be traced in recent publications [7–11].

In the early design stage for the tripod PKMs that are designed for manipulation with high rigidity and high positioning accuracy requirements, stiffness is one of the most overwhelming concerns. However, due to the complex kinematics and structural features, the derivation for the stiffness matrix of such kinds of PKM modules is nevertheless, a tough task, not mentioning the challenge of estimating stiffness throughout the workspace with accuracy and efficiency. Therefore, the estimation for rigidity performance of a tripod PKM still remains as a challenge unless a computational efficient as well as accurate stiffness modeling method is proposed.

Numerous efforts have been contributed to the stiffness modeling and estimation for various PKMs in the past decades. Among all these efforts, the finite element method (FEM) [12, 13], the matrix structure method (MSM) [14, 15], the virtual joint method (VJM) [16–18] and the screw-based method (SBM) [19–22] are the most common used approaches. For example, Pham and his co-workers [13] proposed an analytical finite element model for a flexure parallel mechanism. The analytical results were then compared with the experimental tests to validate the computation accuracy of the proposed stiffness model. As to the matrix structure method, a Jacobian-based stiffness model [15] was proposed by Bi and his co-workers. By using the lumped-parameter method, Zhang et al. [16] established a kinetostatic model for an enhanced tripod mechanism. Li and Xu [19] employed the screw theory to develop a systematic and analytical stiffness model for a family of 3-DOF parallel mechanisms with three prismatic limbs. Wang et al. [22] presented a semi-analytical approach to investigate the stiffness of a tripod-based robot named the TriVariant-B.

It is worth noting that the above stiffness models were specially established for specific PKMs. In other words, it lacks of versatility for these stiffness models being applied to different types of tripod PKMs. Motivated by this thought, the authors aim to present a general stiffness modelling methodology for different types of tripod PKMs with prismatic actuators. To achieve an acceptable balance between the computational efficiency and accuracy, a kinetostatic model that considers the compliances of both limbs and joints is adopted in the present study. For this purpose, the limbs are modeled as spatial beams with corresponding cross-sections constrained by passive joints which are simplified as lumped virtual spring units with equivalent stiffness coefficients.

The reminder of the paper is organized as follows. In Sect. 2, a general kinetostatic stiffness model is established to yield an analytical formulation of the platform's stiffness for the tripod PKMs. In Sect. 3, a general algorithm principle of numerical simulation is proposed to estimate the stiffness performance of two types of tripod PKMs. The stiffness mapping of the two typical tripods are predicted and discussed in details. Finally, some conclusions and remarks are drawn in Sect. 4.

2 Stiffness Modeling Methodology

2.1 Kinematic Definitions

Figure 1 shows the schematic diagram of a general tripod PKM consisting of a platform, a base and three prismatic actuated kinematic limbs. Each limb connects the platform to the base through two passive joints whose geometric centers are denoted as A_i and B_i (i=1, 2, 3), respectively.

As depicted in Fig. 1, the following Cartesian coordinate systems are defined: a global coordinate system B-xyz is attached to the base with its origin B being recommended to set at the geometric center of the base; similarly, a body-fixed coordinate system A-uvw is defined at the platform; and three body-fixed limb reference frames B_i-$x_iy_iz_i$ are arranged at the geometric centers of passive joints B_i. For the convenient of formulation, let z_i point in the direction of vector from B_i to A_i.

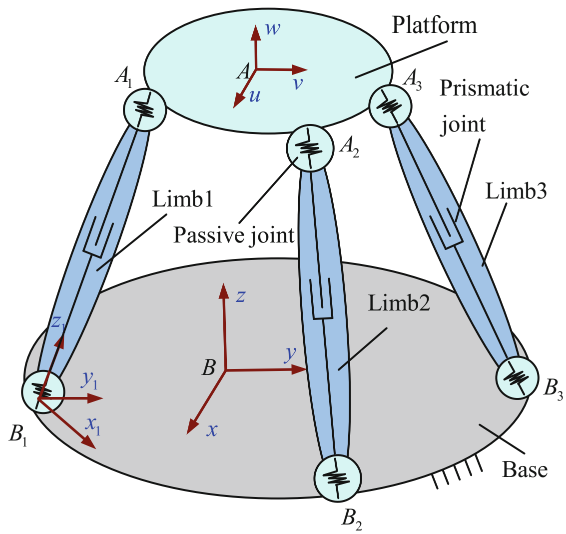

Fig. 1 Schematic diagram of a general tripod PKM

Assume the transformation matrix of A-uvw with respect to B-xyz is ${}^{B}\boldsymbol{T}_{A}$

$$ {}^{B}\boldsymbol{T}_{A} : \mathrm{Trans}(A - uvw \rightarrow B - xyz) \tag{1} $$

Similarly, assume the transformation matrix of B_i-$x_iy_iz_i$ with respect to B-xyz is ${}^{B}\boldsymbol{T}_{Bi}$

$$ {}^{B}\boldsymbol{T}_{Bi} : \mathrm{Trans}(B_i - x_iy_iz_i \rightarrow B - xyz) \tag{2} $$

2.2 Finite Element Formulation of the Limb Assemblage

According to the kinematic motion of limbs in a tripod PKM, they can be roughly classified into two categories, i.e., Case A and Case B.

Figure 2 shows the assembling scheme of Case A where the limb length between the two passive joints is a constant value when the limb undergoes kinematic motions.

In this case, the limb body is constrained by the two passive joints at A_i and B_i through the front bearing and the rear bearing, respectively. The passive joints in the limb assemblage are simplified into two sets of 6-DOF lumped virtual spring units with equivalent linear/angular stiffness constants denoting as $\boldsymbol{k}_{A1i}/\boldsymbol{k}_{A2i}$ and $\boldsymbol{k}_{B1i}/\boldsymbol{k}_{B2i}$. These spring constants can be determined either by finite element computation or by semi-analytical analyses. With the finite element method, the limb can be meshed into finite elements with each node having three linear and three angular coordinates along and about three perpendicular axes [23].

To facilitate the formulation, assume each limb body is divided into n elements with A_i and B_i being one node of the 1st and the nth beam element, respectively. For clarity, one may denote the element nodes in the discrete spatial beam as $e_{i1}, e_{i2}, \ldots, e_{i(n+1)}$ and define a set of nodal reference frame e_{ij}-$x_{ij}y_{ij}z_{ij}$ at the center of element e_{ij} with its three axes parallel to those in the limb frame B_i-$x_iy_iz_i$. With the boundary conditions aroused from the passive joints, a set of static equilibrium equations for the limb can be formulated in the frame of B_i-$x_iy_iz_i$ as

$$ \boldsymbol{k}_i \boldsymbol{\xi}_i = \boldsymbol{w}_i \tag{3} $$

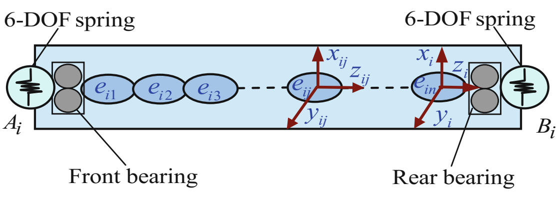

Fig. 2 Assembling scheme and finite element model of an individual limb in Case A

where $\boldsymbol{k}_i$, $\boldsymbol{\xi}_i$ and $\boldsymbol{w}_i$ are the stiffness matrix, the general coordinates and the general load vector of the ith limb body in B_i-$x_iy_iz_i$ and can be further expressed as

$$\boldsymbol{w}_i = [\boldsymbol{f}_{Ai}^T, \boldsymbol{m}_{Ai}^T, \ldots, \boldsymbol{f}_{Bi}^T, \boldsymbol{m}_{Bi}^T]^{\mathrm{T}} \tag{4}$$

where $\boldsymbol{f}_{Ai}/\boldsymbol{m}_A$ and $\boldsymbol{f}_{Bi}/\boldsymbol{m}_{Bi}$ denote the forces/moments acting at the nodes A_i and B_i measured in the B_i-$x_iy_iz_i$, respectively.

The general coordinates of an individual limb measured in the limb frame B_i-$x_iy_iz_i$ can thus be expressed as

$$\boldsymbol{\xi}_i = [\boldsymbol{\delta}_{Ai}^{\mathrm{T}}, \boldsymbol{\rho}_{Ai}^{\mathrm{T}}, \ldots, \boldsymbol{\delta}_{Bi}^{\mathrm{T}}, \boldsymbol{\rho}_{Bi}^{\mathrm{T}}]^{\mathrm{T}} \tag{5}$$

where $\boldsymbol{\delta}_{Ai}/\boldsymbol{\rho}_{Ai}$, $\boldsymbol{\delta}_{Bi}/\boldsymbol{\rho}_{Bi}$ are the linear/angular nodal coordinates of nodes A_i and B_i, respectively.

Therefore, the nodal coordinates of A_i and B_i can be referred to $\boldsymbol{\xi}_i$ by the following transformation matrices

$$\boldsymbol{\delta}_{Ai} = \boldsymbol{N}_{Bi}^{A1}\boldsymbol{\xi}_i, \quad \boldsymbol{\rho}_{Ai} = \boldsymbol{N}_{Bi}^{A2}\boldsymbol{\xi}_i \tag{6}$$

$$\boldsymbol{\delta}_{Bi} = \boldsymbol{N}_{Bi}^{B1}\boldsymbol{\xi}_i, \quad \boldsymbol{\rho}_{Bi} = \boldsymbol{N}_{Bi}^{B2}\boldsymbol{\xi}_i \tag{7}$$

$$\boldsymbol{N}_{Bi}^{A1} = [\mathbf{I}\ \mathbf{0}\ \underbrace{\mathbf{0}\ldots\mathbf{0}}_{6n}], \quad \boldsymbol{N}_{Bi}^{A2} = [\mathbf{0}\ \mathbf{I}\ \underbrace{\mathbf{0}\ldots\mathbf{0}}_{6n}] \tag{8}$$

$$\boldsymbol{N}_{Bi}^{B1} = [\underbrace{\mathbf{0}\ldots\mathbf{0}}_{6n}\ \mathbf{I}\ \mathbf{0}], \quad \boldsymbol{N}_{Bi}^{B2} = [\underbrace{\mathbf{0}\ldots\mathbf{0}}_{6n}\ \mathbf{0}\ \mathbf{I}] \tag{9}$$

where $\mathbf{0}$ and $\mathbf{I}$ denote a zero matrix and an identity matrix in 3×3, respectively.

Figure 3 shows the assembling scheme of Case B where the limb length between the two passive joints is a varying value when the limb undergoes kinematic motions.

Similar to the derivation in Case A, one may assume each limb is divided into n elements with A_i, B_i and C_i being the 1st, the $(j + 1)$th and the $(n + 1)$th nodes of the limb, respectively. Accordingly, a set of equilibrium equations of the ith limb in frame B_i-$x_iy_iz_i$ can be formulated in the matrix form as Eq. (3).

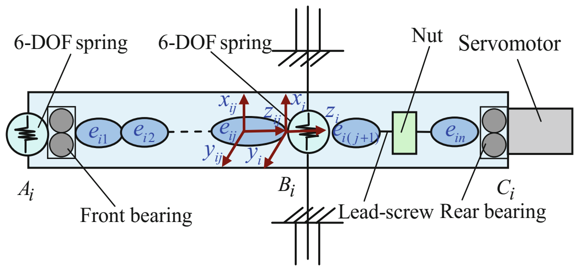

Fig. 3 Assembling scheme and finite element model of an individual limb in Case B

In this case, $\boldsymbol{w}_i$ and $\boldsymbol{\xi}_i$ can be expressed as

$$\boldsymbol{w}_i = [\boldsymbol{f}_{Ai}^{\mathrm{T}}, \boldsymbol{m}_{Ai}^{\mathrm{T}}, \ldots \boldsymbol{f}_{Bi}^{\mathrm{T}}, \boldsymbol{m}_{Bi}^{\mathrm{T}}, \ldots \boldsymbol{f}_{Ci}^{\mathrm{T}}, \boldsymbol{m}_{Ci}^{\mathrm{T}}]^{\mathrm{T}}, \quad \boldsymbol{\xi}_i = \left[\boldsymbol{\delta}_{Ai}^{\mathrm{T}}, \boldsymbol{\rho}_{Ai}^{\mathrm{T}}, \ldots, \boldsymbol{\delta}_{Bi}^{\mathrm{T}}, \boldsymbol{\rho}_{Bi}^{\mathrm{T}}, \ldots, \boldsymbol{\delta}_{Ci}^{\mathrm{T}}, \boldsymbol{\rho}_{Ci}^{\mathrm{T}}\right]^{\mathrm{T}} \tag{10}$$

where $\boldsymbol{f}_{Ci}/\boldsymbol{m}_{Ci}$ denotes the forces/moments acting on the node C_i measured in B_i-$x_i y_i z_i$. $\boldsymbol{\delta}_{Ci}/\boldsymbol{\rho}_{Ci}$ is the three linear/angular nodal coordinates of C_i. The nodal coordinates of A_i, B_i and C_i can be related to $\boldsymbol{\xi}_i$ by the following transformations

$$\boldsymbol{\delta}_{Ai} = \boldsymbol{N}_{Bi}^{A1}\boldsymbol{\xi}_i, \quad \boldsymbol{\rho}_{Ai} = \boldsymbol{N}_{Bi}^{A2}\boldsymbol{\xi}_i \tag{11}$$

$$\boldsymbol{\delta}_{Bi} = \boldsymbol{N}_{Bi}^{B1}\boldsymbol{\xi}_i, \quad \boldsymbol{\rho}_{Bi} = \boldsymbol{N}_{Bi}^{B2}\boldsymbol{\xi}_i \tag{12}$$

$$\boldsymbol{\delta}_{Ci} = \boldsymbol{N}_{Bi}^{C1}\boldsymbol{\xi}_i, \quad \boldsymbol{\rho}_{Ci} = \boldsymbol{N}_{Bi}^{C2}\boldsymbol{\xi}_i \tag{13}$$

$$N_{Bi}^{A1} = [\mathbf{I}\,\mathbf{0}\,\underbrace{\mathbf{0}\ldots\mathbf{0}}_{6n}], \quad N_{Bi}^{A2} = [\mathbf{0}\,\mathbf{I}\,\underbrace{\mathbf{0}\ldots\mathbf{0}}_{6n}] \tag{14}$$

$$\begin{gathered} \boldsymbol{N}_{Bi}^{B1} = \left[\underbrace{\mathbf{0} \quad \ldots \quad \mathbf{0}}_{6j} \quad \mathbf{I} \quad \mathbf{0} \quad \underbrace{\mathbf{0} \quad \ldots \quad \mathbf{0}}_{6(n-j)}\right], \\ \boldsymbol{N}_{Bi}^{B2} = \left[\underbrace{\mathbf{0} \quad \ldots \quad \mathbf{0}}_{6j} \quad \mathbf{0} \quad \mathbf{I} \quad \underbrace{\mathbf{0} \quad \ldots \quad \mathbf{0}}_{6(n-j)}\right] \end{gathered} \tag{15}$$

$$\boldsymbol{N}_{Bi}^{C1} = \left[\underbrace{\mathbf{0} \quad \ldots \quad \mathbf{0}}_{6n} \quad \mathbf{I} \quad \mathbf{0}\right], \quad \boldsymbol{N}_{Bi}^{C2} = \left[\underbrace{\mathbf{0} \quad \ldots \quad \mathbf{0}}_{6n} \quad \mathbf{0} \quad \mathbf{I}\right] \tag{16}$$

Equation (3) can be transformed into the global coordinate system B-xyz as

$$\boldsymbol{K}_i\boldsymbol{U}_i = \boldsymbol{W}_i \tag{17}$$

where $\boldsymbol{K}_i$, $\boldsymbol{U}_i$ and $\boldsymbol{W}_i$ are the stiffness matrix, the general coordinates vector and the external loads vector of limb i measured in B-xyz. And there exist

$$\boldsymbol{K}_i = \boldsymbol{T}_i\boldsymbol{k}_i\boldsymbol{T}_i^{\mathrm{T}}, \quad \boldsymbol{U}_i = \boldsymbol{T}_i\xi_i, \quad \boldsymbol{W}_i = \boldsymbol{T}_i\boldsymbol{w}_i \tag{18}$$

$$\boldsymbol{T}_i = \mathrm{diag}[{}^{B}\boldsymbol{T}_{Bi}, {}^{B}\boldsymbol{T}_{Bi}, \ldots, {}^{B}\boldsymbol{T}_{Bi}, {}^{B}\boldsymbol{T}_{Bi}] \tag{19}$$

where ${}^{B}\boldsymbol{T}_{Bi}$ is the transformation matrix of B_i-$x_i y_i z_i$ with respect to B-xyz as defined in Eq. (2) and can be determined by inverse kinematics.

2.3 Equilibrium Equation of the Platform

The force diagram of the platform is depicted in Fig. 4. Herein, $\boldsymbol{F}_{Ai}/\boldsymbol{M}_{Ai}$ denotes the forces/moments provided by the passive joints A_i; $\boldsymbol{F}_{\mathrm{P}}/\boldsymbol{M}_{\mathrm{P}}$ represents the external forces/moments acting on the platform.

With the Newton's 2nd law, the following static equations can be formulated

$$-\sum \boldsymbol{F}_{Ai} + \boldsymbol{F}_{\mathrm{P}} = \boldsymbol{0}, -\sum \boldsymbol{r}_{Ai} \times \boldsymbol{F}_{Ai} + \boldsymbol{srritrmsrritrmM}_{\mathrm{P}} - \sum \boldsymbol{M}_{Ai} = \boldsymbol{0} \tag{20}$$

$$\boldsymbol{F}_{Ai} = {}^{B}\boldsymbol{T}_{Bi}\boldsymbol{f}_{Ai}, \quad \boldsymbol{M}_{Ai} = {}^{B}\boldsymbol{T}_{Bi}\boldsymbol{m}_{Ai} \tag{21}$$

where $\boldsymbol{r}_{Ai}$ is the vector pointing from A to A_i measured in B-xyz.

2.4 Deformation Compatibility Conditions

The displacement relationships between the platform/base and the limb is depicted in Fig. 5, in which $A_{i\mathrm{M}}$ and $A_{i\mathrm{L}}$ denote the interface points associated with the platform and the ith limb, while $B_{i\mathrm{B}}$ and $B_{i\mathrm{L}}$ denote the interface points associated with the base and the ith limb, respectively. $\nabla\boldsymbol{A}_i/\boldsymbol{\delta A}_i$ and $\boldsymbol{\delta B}_i/\boldsymbol{\rho}_{Bi}$ are the linear/angular displacements of $A_{i\mathrm{M}}$ and $B_{i\mathrm{L}}$ measured in the limb coordinate system B_i-$x_iy_iz_i$.

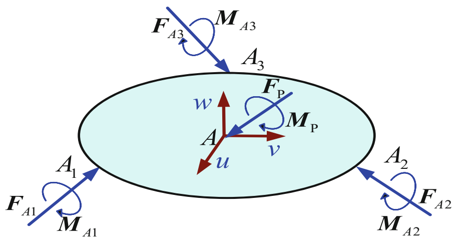

Fig. 4 Force diagram of the platform

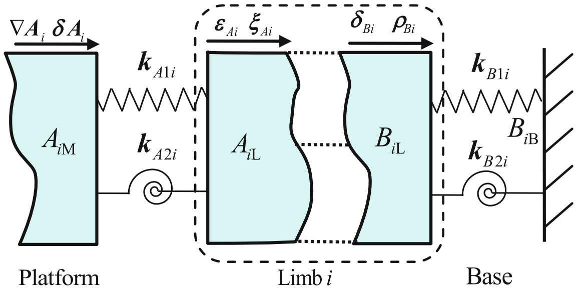

Fig. 5 Two types of deformation compatibility conditions

Assume the elastic motion of the platform caused by the deflections of the three flexible limb assemblages is $\boldsymbol{U}_{\mathrm{P}}$, the elastic displacements of $A_{i\mathrm{M}}$ (attached to the platform) can be derived as the followings.

$$\nabla \boldsymbol{A}_i = {}^{B}\boldsymbol{T}_{Bi}^{T}\boldsymbol{D}^{ri}\boldsymbol{U}_{\mathrm{P}}, \quad \delta \boldsymbol{A}_i = {}^{B}\boldsymbol{T}_{Bi}^{\mathrm{T}}\boldsymbol{D}^{ai}\boldsymbol{U}_{\mathrm{P}} \tag{22}$$

$$\boldsymbol{D}^{ri} = \begin{bmatrix} 1 & 0 & 0 & 0 & z_{Ai} & -y_{Ai} \\ 0 & 1 & 0 & -z_{Ai} & 0 & x_{Ai} \\ 0 & 0 & 1 & y_{Ai} & -x_{Ai} & 0 \end{bmatrix}, \quad \boldsymbol{D}^{ai} = \begin{bmatrix} \mathbf{0}_{3\times 3} & \mathbf{I}_{3\times 3} \end{bmatrix} \tag{23}$$

where x_{Ai}, y_{Ai} and z_{Ai}, are the coordinates of point A_i measured in B-xyz.

As a result, the reaction forces and moments of the passive joints A_i and B_i measured in B_i-$x_iy_iz_i$ can be obtained as

$$\boldsymbol{f}_{Ai} = -\boldsymbol{k}_{A1i}\left(\boldsymbol{N}_{Bi}^{A1}\boldsymbol{T}_i^{\mathrm{T}}\boldsymbol{U}_i - {}^{B}\boldsymbol{T}_{Bi}^{\mathrm{T}}\boldsymbol{D}^{ri}\boldsymbol{U}_{\mathrm{P}}\right), \quad \boldsymbol{m}_{Ai} = -\boldsymbol{k}_{A2i}\left(\boldsymbol{N}_{Bi}^{A2}\boldsymbol{T}_i^{\mathrm{T}}\boldsymbol{U}_i - {}^{B}\boldsymbol{T}_{Bi}^{\mathrm{T}}\boldsymbol{D}^{ai}\boldsymbol{U}_{\mathrm{P}}\right) \tag{24}$$

$$\boldsymbol{f}_{Bi} = -\boldsymbol{k}_{B1i}\boldsymbol{N}_{Bi}^{B1}\boldsymbol{T}_i^{\mathrm{T}}\boldsymbol{U}_i, \quad \boldsymbol{m}_{Bi} = -\boldsymbol{k}_{B2i}\boldsymbol{N}_{Bi}^{B2}\boldsymbol{T}_i^{\mathrm{T}}\boldsymbol{U}_i \tag{25}$$

2.5 *Stiffness Matrix of the Platform*

By assembling the equilibrium equations of the limbs and the platform, one may derive the governing equations of a general tripod PKM in the matrix form as

$$\boldsymbol{K}\boldsymbol{U} = \boldsymbol{W} \tag{26}$$

where $\boldsymbol{K}$, $\boldsymbol{U}$ and $\boldsymbol{W}$ are the governing stiffness matrix; coordinates vector and load vector. And there exist

$$\boldsymbol{K} = \begin{bmatrix} \boldsymbol{K}_{1,1} & & & \boldsymbol{K}_{1,4} \\ & \boldsymbol{K}_{2,2} & & \boldsymbol{K}_{2,4} \\ & & \boldsymbol{K}_{3,3} & \boldsymbol{K}_{3,4} \\ \boldsymbol{K}_{4,1} & \boldsymbol{K}_{4,2} & \boldsymbol{K}_{4,3} & \boldsymbol{K}_{4,4} \end{bmatrix} \tag{27}$$

$$\boldsymbol{U} = \begin{bmatrix} \boldsymbol{U}_1^{\mathrm{T}} & \boldsymbol{U}_2^{\mathrm{T}} & \boldsymbol{U}_3^{\mathrm{T}} & \boldsymbol{U}_{\mathrm{P}}^{\mathrm{T}} \end{bmatrix}^{\mathrm{T}} \tag{28}$$

$$\boldsymbol{W} = \begin{bmatrix} \boldsymbol{W}_1^{\mathrm{T}} & \boldsymbol{W}_2^{\mathrm{T}} & \boldsymbol{W}_3^{\mathrm{T}} & \boldsymbol{W}_{\mathrm{P}}^{\mathrm{T}} \end{bmatrix}^{\mathrm{T}}, \quad \boldsymbol{W}_{\mathrm{P}} = \begin{bmatrix} \boldsymbol{F}_{\mathrm{P}}^{\mathrm{T}} & \boldsymbol{M}_{\mathrm{P}}^{\mathrm{T}} \end{bmatrix}^{\mathrm{T}} \tag{29}$$

The stiffness matrix of the platform expressed in the body-fixed frame A-uvw can be further formulated as

$$\boldsymbol{K}_{\mathrm{p}}=\boldsymbol{T}_0^{\mathrm{T}}\{[\boldsymbol{K}^{-1}]_{(H-18(n+1))\times(H-18(n+1))}\}^{-1}\boldsymbol{T}_0,\quad \boldsymbol{T}_0=\mathrm{diag}\left[{}^{B}\boldsymbol{T}_A\quad {}^{B}\boldsymbol{T}_A\right] \tag{30}$$

where H=18n + 24 is the dimension of the governing stiffness matrix.

3 Stiffness Estimation

In this section, two typical tripod PKMs, namely the Sprint Z3 head module (Case A) and the A3 head module (Case B) are taken as examples to demonstrate the versatility of the proposed general stiffness modeling methodology. The stiffness mapping of the two example systems over a typical work plane is plotted and briefly discussed.

The structures of the two example tripods are depicted in Fig. 6.

As can be observed from Fig. 6, the topological architecture behind the two tripods are a 3-$\underline{\text{P}}$RS parallel mechanism and a 3-R$\underline{\text{P}}$S parallel mechanism, respectively [24, 25].

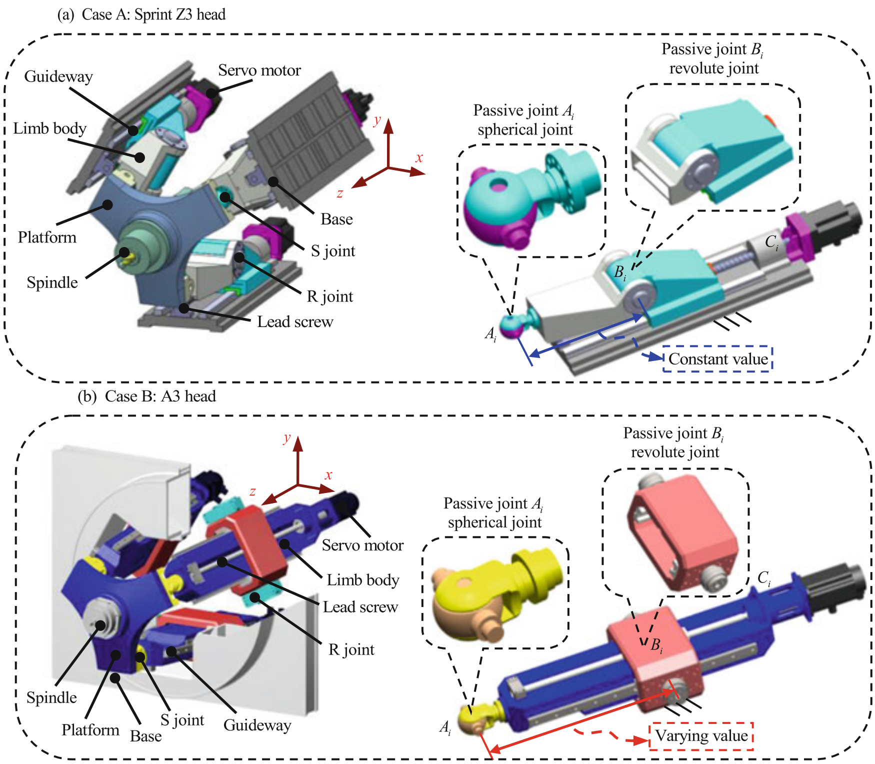

Fig. 6 Structures of two typical tripods

The major geometric parameters and stiffness coefficients of the two typical tripods are listed in Table 1.

Based on the above parameters and the derivations described in Sect. 2, one can obtain the stiffness mapping of the two tripods throughout the workspace. For the sake of generality, the following illustrates the mappings of the six principle stiffness values over a given typical work plane of $p_z = 570$ mm. Herein, p_z denotes the central distance between the base and the platform in z direction; ψ and θ are the Euler angles in terms of precession and nutation; k_{11}, k_{22} and k_{33} denote the three linear principle stiffness values along u, v and w axes while k_{44}, k_{55} and k_{66} represent the three angular principle stiffness values about u, v and w axes.

As shown in Figs. 7 and 8, the stiffness mapping of the two tripods is strongly position-dependent and is coincident with the tripod's structural features. To be specific, the distribution of stiffness values over the work plane for the two tripods are both symmetric with respect to θ, which can be physically explained by the structural symmetry of limb 1, limb 2 and limb 3.

Further observations show that ψ and θ have different impacts on the stiffness distributions of the two tripods. Taking the Sprint Z3 head for instance, the precession ψ has a 'stronger' impact on the linear principle stiffness values along u and v axes, while has a 'weaker' impact on the linear principle stiffness along w axis. In addition, for both the Sprint Z3 head and the A3 head, the stiffness value along

Table 1 Parameters of the Sprint Z3 head and A3 head

Nomenclature	Z3 head	A3 head
Radius of the platform r_p	250	250
Radius of the base r_b	250	250
Stroke of the tripod s	200	200
Elastic modulus of the limb body E	200	200
Shear modulus of the limb body G	80	80
Stiffness of short axis in u direction k_{su}	23	23
Stiffness of short axis in v direction k_{sv}	23	23
Stiffness of short axis in w direction k_{sw}	623	623
Stiffness of long axis in u direction k_{lu}	112	112
Stiffness of long axis in v direction k_{lv}	214	214
Stiffness of long axis in w direction k_{lw}	100	100
Stiffness of cross axis in u direction k_{cu}	676	676
Stiffness of cross axis in v direction k_{cv}	446	446
Stiffness of cross axis in w direction k_{cw}	348	348
Stiffness of a revolute joint along x direction k_{rx}	280	380
Stiffness of a revolute joint along y direction k_{ry}	330	530
Stiffness of a revolute joint along z direction k_{rz}	330	530
Stiffness of a revolute joint about y direction k_{rv}	20	18
Stiffness of a revolute joint about z direction k_{rw}	20	18

Units mm, Gpa, N μm^{-1}, N m rad^{-1}

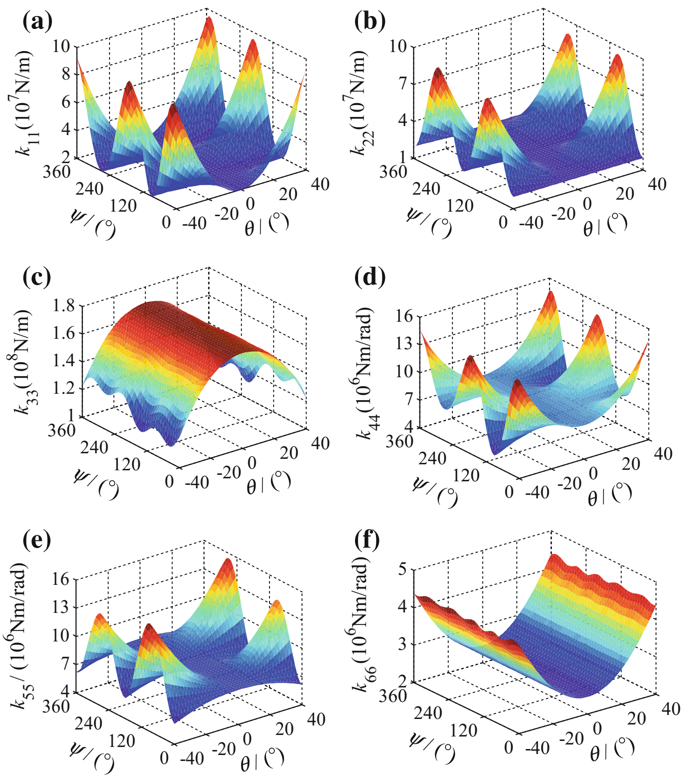

Fig. 7 Six principle stiffness values of the Sprint Z3 head over the work plane of p_z = 570 mm

w axis is the largest among the three linear principle stiffness values and the stiffness value about w axis is the smallest among the three angular principle stiffness values. This may imply that the rigidity performance about w direction must be paid more attention when design and apply these two kinds of tripods.

By comparing Figs. 7 with 8, one can find that the A3 head claims a competitive stiffness performance to the Sprint Z3 head along w axis. However, the rigidities of the A3 head along and about other axes are smaller than those of the Sprint Z3 head.

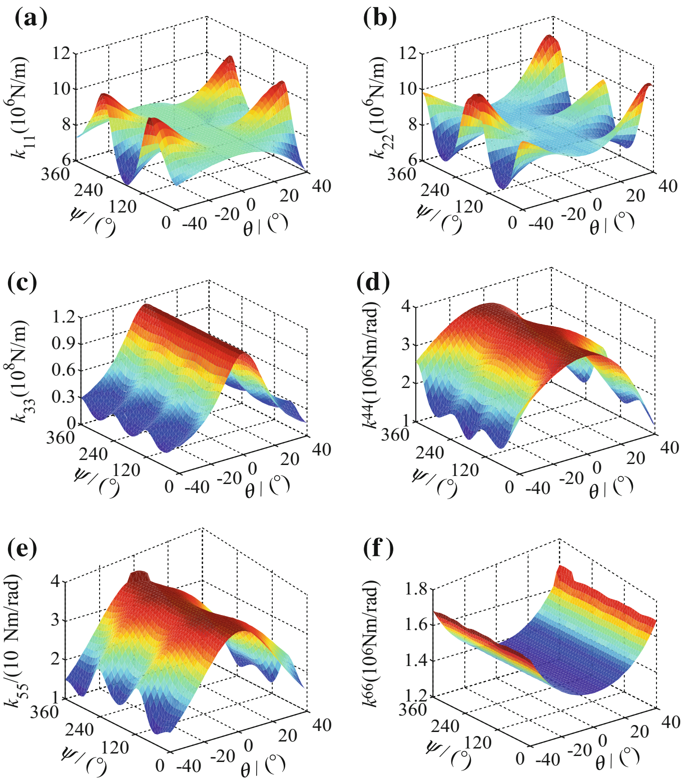

Fig. 8 Six principle stiffness values of the A3 head over the work plane of p_z = 570 mm

4 Conclusions

With the studies carried out in this paper, the following conclusions can be drawn:

(1) The general tripod PKMs are classified into two groups according to the motion patterns of the kinematic limbs. With this classification, a kinetostatic model based methodology is proposed to derive the analytical stiffness matrix of the platform for the general tripod PKMs with prismatic actuators.
(2) The proposed kinetostatic model considers the deflections of limb structures as well as the joint assemblages, leading to a satisfactory computation accuracy of the stiffness property for the tripod's platform.
(3) The stiffness mapping of two typical tripods named the Sprint Z3 head and the A3 head are predicted numerically to show strong position-dependency and structural symmetry.

(4) The present study provides a general framework for the stiffness evaluation of tripod-based PKMs with prismatic actuators. Also it is expected that the present kinetostatic model can be further expanded to an elastodynamic model by adding the mass and coriolis terms, with which the dynamic analyses for the tripods can be conducted.

Acknowledgements This work was supported by the Open Fund of the State Key Laboratory for Manufacturing Systems Engineering (Xi'an Jiaotong University) with Grant No. sklms2015004 and Open Fund of Shanghai Key Laboratory of Digital Manufacture for Thin-walled Structures with Grant No. 2014001. The second author would like to acknowledge for Innovation Research Fund for Postgraduates of Anhui University of Technology (Grant No. 2015032).

References

1. Y. Li, Q. Xu, Kinematic analysis of a 3-PRS parallel manipulator. Robot. Comput.-Integr. Manuf. **23**(4), 395–408 (2007)
2. N. Hennes, D. Staimer, Application of PKM in aerospace manufacturing-high performance machining centers ECOSPEED, ECOSPEED-F and ECOLINER, in *Proceedings of the 4th Chemnitz Parallel Kinematics Seminar* (2004), pp. 557–577
3. Z.M. Bi, Kinetostatic modeling of Exechon parallel kinematic machine for stiffness analysis. Int. J. Adv. Manuf. Technol. **71**(1–4), 325–335 (2014)
4. T. Bonnemains, H. Chanal, B.C. Bouzgarrou et al., Dynamic model of an overconstrained PKM with compliances: The Tripteor X7. Robot. Comput.-Integr. Manuf. **29**(1), 180–191 (2013)
5. Y.G. Li, H.T. Liu, X.M. Zhao et al., Design of a 3-DOF PKM module for large structural component machining. Mech. Mach. Theory **45**(6), 941–954 (2010)
6. Z.J. Tian et al., Dynamic modeling and eigenvalue evaluation of a 3-DOF PKM module. Chin. J. Mech. Eng. **23**(2), 166–173 (2010)
7. Y. Jin, Z. Bi, C. Higgins, et al., Optimal design of a new parallel kinematic machine for large volume machining. *Advances in Reconfigurable Mechanisms and Robots I*, (Springer, London, 2012), pp. 343–354
8. D. Zlatanov, M. Zoppi, R. Molfino, Constraint and singularity analysis of the exechon tripod, in *ASME 2012 International Design Engineering Technical Conferences and Computers and Information in Engineering Conference*, (American Society of Mechanical Engineers, 2012), pp. 679–688
9. Z.M. Bi, Y. Jin, Kinematic modeling of Exechon parallel kinematic machine. Robot. Comput.-Integr. Manuf. **27**(1), 186–193 (2011)
10. X. Chen, X.J. Liu, F.G. Xie et al., A comparison study on motion/force transmissibility of two typical 3-DOF parallel manipulators: the sprint Z3 and A3 tool heads. Int. J. Adv. Rob. Syst. **11**(1), 74–89 (2014)
11. F. Xi, D. Zhang, C.M. Mechefske et al., Global kinetostatic modelling of tripod-based parallel kinematic machine. Mech. Mach. Theory **39**(4), 357–377 (2004)
12. A. Ahmad, K. Andersson, U. Sellgren, S. Khan, A stiffness modeling methodology for simulation-driven design of haptic devices. Eng. Comput. **30**(1), 125–141 (2012)
13. H.H. Pham, I.M. Chen, Stiffness modeling of flexure parallel mechanism. Precision Eng. **29** (4), 467–478 (2005)
14. T. Huang, X. Zhao, D.J. Whitehouse, Stiffness estimation of a tripod-based parallel kinematic machine. IEEE Trans. Robot. Autom. **18**(1), 50–58 (2002)

15. Z.M. Bi, S.Y.T. Lang, D. Zhang, Stiffness analysis of a tripod with a passive link, in *ASME 2005 International Mechanical Engineering Congress and Exposition*, (American Society of Mechanical Engineers, 2005), pp. 1665–1671
16. D. Zhang, L. Wang, Conceptual development of an enhanced tripod mechanism for machine tool. Robot. Comput.-Integr. Manuf. **21**(4), 318–327 (2005)
17. F. Majou, C. Gosselin, P. Wenger et al., Parametric stiffness analysis of the Orthoglide. Mech. Mach. Theory **42**(3), 296–311 (2007)
18. M. Ceccarelli, G. Carbone, A stiffness analysis for CaPaMan (Cassino parallel manipulator). Mech. Mach. Theory **37**(5), 427–439 (2002)
19. Y. Li, Q. Xu, Stiffness analysis for a 3-PUU parallel kinematic machine. Mech. Mach. Theory **43**(2), 186–200 (2008)
20. B. Li, H. Yu, Z. Deng et al., Stiffness modeling of a family of 6-DoF parallel mechanisms with three limbs based on screw theory. J. Mech. Sci. Technol. **24**(1), 373–382 (2010)
21. J.S. Dai, X. Ding, Compliance analysis of a three-legged rigidly-connected platform device. J. Mech. Des. **128**(4), 755–764 (2006)
22. Y.Y. Wang, T. Huang, X.M. Zhao et al., A semi-analytical approach for stiffness modeling of PKM by considering compliance of machine frame with complex geometry. Sci. Bull. **53**(16), 2565–2574 (2008)
23. H. David, *Fundamentals of Finite Element Analysis* (McGraw-Hill, NewYork, 2004)
24. Y.Q. Zhao, J. Zhang, L.Y. Ruan et al., A modified elasto-dynamic model based static stiffness evaluation for a 3-PRS PKM. Proc. Inst. Mech. Eng. Part C J. Mech. Eng. Sci. **230**(3), 353–366 (2016)
25. J. Zhang, Y.Q. Zhao, H.W. Luo, Hybrid-model-based stiffness analysis of a three-revolute-prismatic-spherical parallel kinematic machine. Proc. Inst. Mech. Eng. Part B J. Eng. Manuf. doi:10.1177/0954405416634257(2016)